

1 Genome wide association study of behavioral, physiological and 2 gene expression traits in a multigenerational mouse intercross

3 Authors

4 Natalia M. Gonzales¹
5 Jungkyun Seo^{1,2,3}
6 Ana Isabel Hernandez-Cordero⁴
7 Celine L. St. Pierre^{1,5}
8 Jennifer S. Gregory⁴
9 Margaret G. Distler¹
10 Mark Abney¹
11 Stefan Canzar^{1,8}
12 Arimantas Lionikas⁴
13 Abraham A. Palmer^{1,6,7}

14 Affiliations

15 1. Department of Human Genetics, University of Chicago, Chicago, IL 60637, USA
16 2. Computational Biology & Bioinformatics Graduate Program, Duke University, Durham, NC, 27708, USA
17 3. Center for Genomic & Computational Biology, Duke University, Durham, NC, 27708, USA
18 4. School of Medicine, Medical Sciences and Nutrition, College of Life Sciences and Medicine, University of Aberdeen,
19 Aberdeen, UK
20 5. Department of Genetics, Washington University School of Medicine, St. Louis, MO 63108, USA
21 6. Department of Psychiatry, University of California San Diego, La Jolla, CA 92093, USA
22 7. Institute for Genomic Medicine, University of California San Diego, La Jolla, CA 92093, USA
23 8. Gene Center, Ludwig-Maximilians-Universität München, 81377 Munich, Germany

24
25 Correspondence should be addressed to A.A.P (aapalmer@ucsd.edu)
26 ORCID: orcid.org/0000-0003-3634-0747

27 Author contributions

28 NMG maintained the AIL colony, phenotyped the mice, prepared RNA-sequencing libraries, and performed QTL/eQTL
29 analysis under supervision of AAP and MA. AAP and MA also provided computational resources for the analyses in
30 this paper. JS prepared RNA-sequencing data for eQTL mapping under supervision of SC. CLS assisted with colony
31 maintenance, tissue collection, RNA extraction, and GBS library preparation. MGD performed experiments in mutant
32 mice. AL, JSG and AIHC measured hind limb muscle and bone phenotypes. NMG co-wrote the manuscript with AAP,
33 who designed the study.

34 Funding

35 Research reported in this publication was funded by NIDA (R01DA021336 awarded to AAP) and NIAMS
36 (R01AR056280 awarded to AL). We also received support from NIGMS (NMG: T32GM007197 and MGD:
37 T32GM07281), NIDA (NMG: F31DA03635803), NHGRI (MA: R01HG002899), and the IMS Elphinstone Scholarship at
38 the University of Aberdeen (AIHC). The content is solely the responsibility of the authors and does not necessarily
39 represent the official views of the NIH. The authors declare no conflict of interest.

40 Acknowledgements

41 We would like to recognize Clarissa Parker for exceptional mentorship and for training NMG in mouse behavioral
42 research and husbandry. We are grateful to Heather Lawson at the Washington University in St. Louis for providing
43 LG/J and SM/J genome sequences. We thank the Gilad Lab and Functional Genomics Facility at the University of
44 Chicago for generating DNA- and RNA-seq data. We wish to acknowledge outstanding technical assistance from Mike
45 Jarsulic at the Biological Sciences Division Center for Research Informatics at the University of Chicago and Apurva
46 Chitre at UCSD. Finally, we thank John Novembre, Graham McVicker, Joe Davis, Peter Carbonetto and Shyam
47 Gopalakrishnan for advice regarding GBS, RNA-seq, and statistical analysis.

48 Abstract

49 Genome wide association analyses (**GWAS**) in model organisms have numerous advantages compared to human
50 GWAS, including the ability to use populations with well-defined genetic diversity, the ability to collect tissue for gene
51 expression analysis and the ability to perform experimental manipulations. We examined behavioral, physiological, and
52 gene expression traits in 1,063 male and female mice from a 50-generation intercross between two inbred strains
53 (LG/J and SM/J). We used genotyping by sequencing in conjunction with whole genome sequence data from the two
54 founder strains to obtain genotypes at 4.3M SNPs. As expected, all alleles were common (mean MAF=0.35) and
55 linkage disequilibrium degraded rapidly, providing excellent power and sub-megabase mapping precision. We
56 identified 126 genome-wide significant loci for 50 traits and integrated this information with 7,081 *cis*-eQTLs and 1,476
57 *trans*-eQTLs identified in hippocampus, striatum and prefrontal cortex. We replicated several loci that were identified
58 using an earlier generation of this intercross, including an association between locomotor activity and a locus
59 containing a single gene, *Csmd1*. We also showed that *Csmd1* mutant mice recapitulated the locomotor phenotype.
60 Our results demonstrate the utility of this population, identify numerous novel associations, and provide examples of
61 replication in an independent cohort, which is customary in human genetics, and replication by experimental
62 manipulation, which is a unique advantage of model organisms.

63 Introduction

64 Genome-wide association studies (**GWAS**) have revolutionized psychiatric genetics; however, they have also
65 presented numerous challenges. Some of these challenges can be addressed by using model organisms. For
66 example, human GWAS are confounded by environmental variables, such as childhood trauma, which can reduce
67 power to detect genetic associations. In model organisms, environmental variables can be carefully controlled.
68 Furthermore, it has become clear that phenotypic variation in humans is due to numerous common and rare variants of
69 small effect. In model organisms, genetic diversity can be controlled such that all variants are common. In addition,
70 allelic effect sizes in model organisms are dramatically larger than in humans^{1,2}. Furthermore, because the majority of
71 associated loci are in noncoding regions, expression quantitative trait loci (**eQTLs**) are useful for elucidating underlying
72 molecular mechanisms^{3,4}. However, it remains challenging to obtain large, high quality samples of human tissue,
73 particularly from the brain. In contrast, tissue for gene expression studies can be collected from model organisms
74 under optimal conditions. Finally, the genomes of model organisms can be edited to assess the functional
75 consequences of specific mutations.

76
77 Model organism GWAS often employ multigenerational intercrosses because they promote recombination of ancestral
78 haplotypes. We used an advanced intercross line (**AIL**) of mice, which is the simplest possible multigenerational
79 intercross. AILs, originally proposed by Darvasi and Soller in 1995 (ref. 5), are produced by intercrossing two inbred
80 strains beyond the F2 generation. Because the two inbred strains contribute equally to an AIL, all variants are
81 common, and alleles that are identical by state are necessarily identical by descent (**IBD**), which greatly simplifies
82 phasing and imputation. We performed a GWAS using the world's most advanced mouse AIL, which was created over
83 50 generations ago by crossing the LG/J (**LG**) and SM/J (**SM**) inbred strains⁶. We investigated over 100 traits using
84 mice from generations 50-56 (**G50-56**), including locomotor activity, response to methamphetamine, prepulse inhibition
85 (**PPI**), body weight, and various muscle and bone phenotypes. We also sequenced mRNA from three brain regions
86 and used those data to map eQTLs and identify quantitative trait genes (**QTGs**) at each locus. Finally, we explored
87 replication of previous associations identified in LG x SM G34⁷⁻¹¹ and used mutant mice to test one of our strongest
88 candidate QTGs.

89 Results

90 We used genotyping by sequencing (**GBS**) to genotype 1,063 of the 1,123 mice that were phenotyped (60 were not
91 successfully genotyped for technical reasons described in the **Supplementary Note**). After quality control, GBS
92 yielded 38,238 autosomal SNPs. In the 24 AIL mice that were also genotyped on the Giga Mouse Universal
93 Genotyping Array (**GigaMUGA**)¹², only 24,934 markers were polymorphic in LG and SM (**Supplementary Fig.1**). LG
94 and SM have been re-sequenced¹³, which allowed us to impute AIL genotypes at ~4.3 million single nucleotide
95 polymorphisms (**SNPs**; **Fig. 1a**). Consistent with the expectation for an AIL, the average minor allele frequency (**MAF**)
96 was high (**Fig. 1b**). Linkage disequilibrium (**LD**) decay, which is critical to mapping resolution, has improved since LG x
97 SM G34 (**Fig. 1c**)⁷.

98

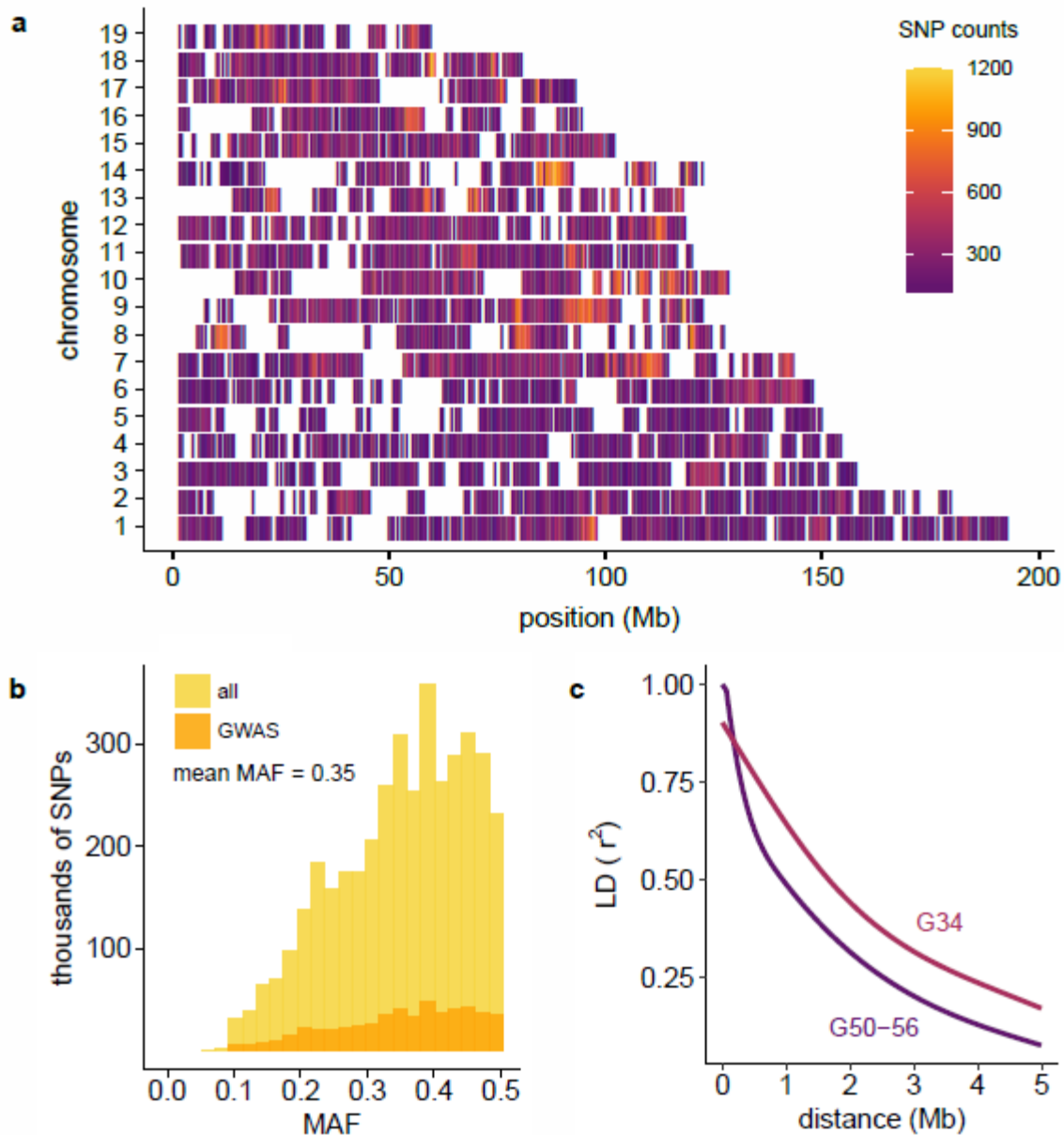
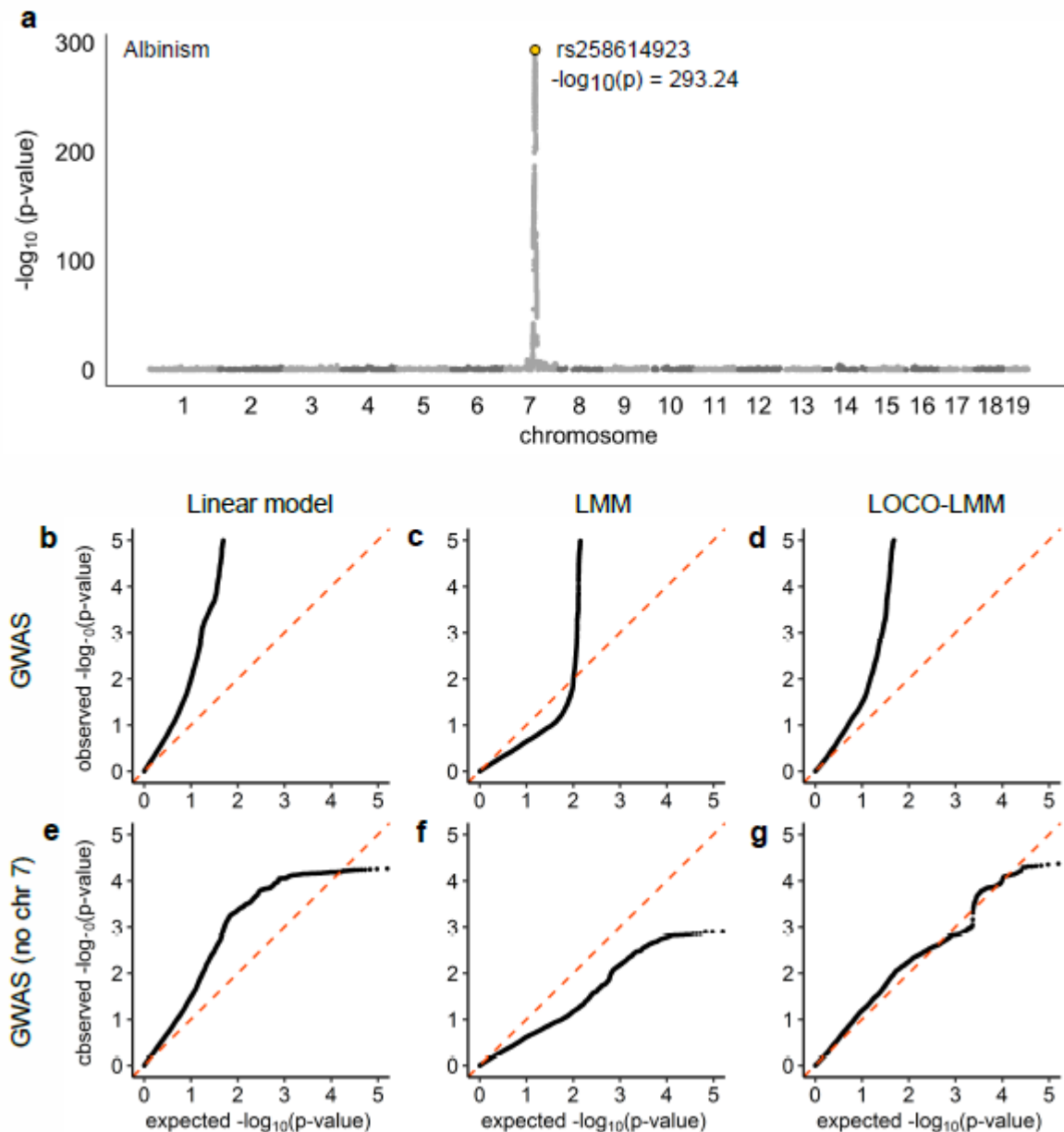


Figure 1. SNPs, minor allele frequencies (MAFs) and linkage disequilibrium (LD) decay in the LG x SM AIL. Imputation provided ~4.3 million SNPs. Filtering for LD ($r^2 \geq 0.95$), MAF < 0.1 , and HWE ($p \leq 7.62 \times 10^{-6}$) resulted in 523,028 SNPs for GWAS. **(a)** SNP distribution and density of GWAS SNPs are plotted in 500 kb windows for each chromosome. As shown in **Supplementary Fig. 1**, regions with low SNP density correspond to regions predicted to be nearly IBD in LG and SM (Nikolskiy *et al.* 2015). **(b)** MAF distributions are shown for ~4.3 million imputed SNPs (gold; unfiltered) and for the 523,028 SNPs used for GWAS (orange; filtered). Mean MAF is the same in both SNP sets. **(c)** Comparison of LD decay in G50-56 (dark purple) and G34 (light purple) of the LG x SM AIL. Each curve was plotted using the 95th percentile of r^2 values for SNPs spaced up to 5 Mb apart.

LOCO-LMM effectively reduces the type II error rate

Linear mixed models (LMMs) are commonly used to perform GWAS in AILs and other populations that include close relatives¹⁴. SNP data are used to obtain a genetic relationship matrix (GRM); however, this can lead to an inflation of the type II error rate due to proximal contamination^{15,16}. We previously proposed using a leave-one-chromosome-out LMM (LOCO-LMM) to address this issue¹⁵. To demonstrate the appropriateness of a LOCO-LMM, we performed a GWAS for albinism, which is a recessive Mendelian trait, using three approaches: a simple linear model, an LMM and a LOCO-LMM (**Fig. 2**). GWAS using a LOCO-LMM for albinism yielded an association on chromosome 7 (**Fig. 2a**); accurately identifying the albino locus (*Tyr*). As expected, p-values from a genome-wide scan using a linear model, which does not account for relatedness, appeared highly inflated (**Fig. 2b**). This inflation was greatly reduced by fitting a standard LMM, which included SNPs from chromosome 7 in both the fixed and random effects (**Fig. 2c**). The LOCO-LMM, which does not include SNPs from the chromosome being tested in the GRM, showed an intermediate level of inflation (**Fig. 2d**). Was the inflation observed in **Fig. 2b-d** due to true signal, or uncontrolled population structure? To

119 address this question, we repeated these analyses after excluding SNPs on chromosome 7 from the fixed effect (**Fig.**
 120 **2e-g**). Even in the absence of the causal locus, the simple linear model showed substantial inflation, which can only be
 121 explained by population structure (**Fig. 2e**). The standard LMM appeared overly conservative, which we attributed to
 122 proximal contamination (**Fig. 2f**). The LOCO-LMM showed no inflation, consistent with the absence of *Tyr* and linked
 123 SNPs in the fixed effect (**Fig. 2g**). These results demonstrate the appropriateness of a LOCO-LMM.



124
 125
 126
 127
 128
 129
 130
 131
 132

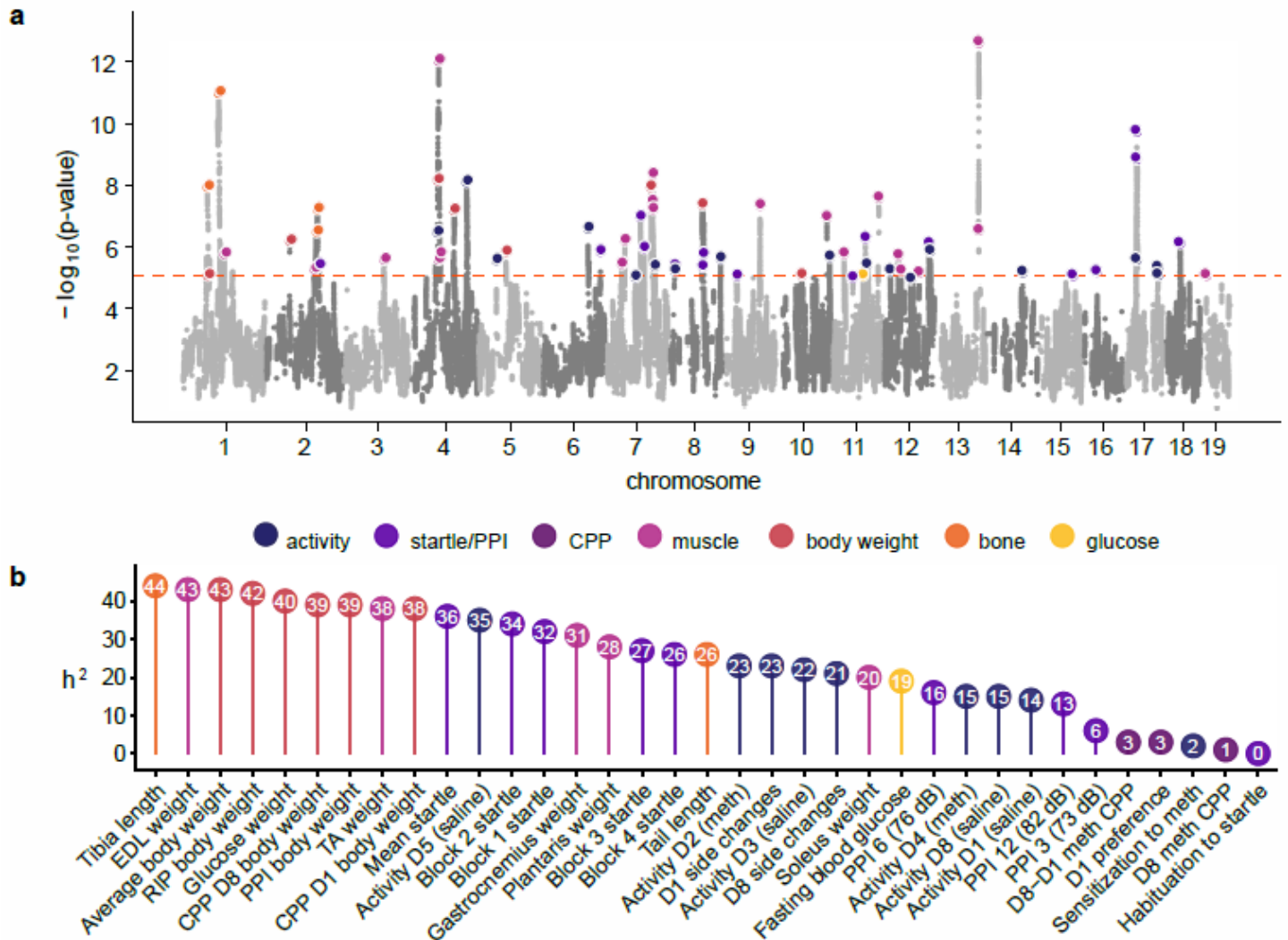
Figure 2. GWAS for albinism verifies that the LOCO-LMM effectively controls type I and type II error. We conducted a GWAS for albinism, a Mendelian trait caused by the *Tyr* locus on mouse chromosome 7, using three models: a linear model, an LMM, and a LOCO-LMM. We also repeated each scan after excluding SNPs on chromosome 7. A Manhattan plot of results from the LOCO-LMM is shown in (a). Quantile-quantile plots of expected vs. observed p-values are shown for (b) a simple linear model that does not account for relatedness; (c) a standard LMM that includes all GWAS SNPs in the genetic relatedness matrix (**GRM**; i.e. the random effect); and (d) a LOCO-LMM whose GRM excludes SNPs located on the chromosome being tested. Plots (e-g) show results after excluding chromosome 7 from the GWAS.

133 Genetic architecture of complex traits in the LG x SM AIL

134 We used an LD-pruned set of 523,028 autosomal SNPs genotyped in 1,063 mice from LG x SM G50-56 to perform
 135 GWAS for 120 behavioral and physiological traits using a LOCO-LMM (**Fig. 3a**). We used permutation to define a
 136 significance threshold of $p=8.06 \times 10^{-6}$ ($\alpha=0.05$). There were 52 loci associated with 33 behavioral traits and 74 loci
 137 associated with 17 physiological traits (**Fig. 3a, Supplementary Table 1; Supplementary Fig. 2**).

138
139
140
141
142
143
144
145
146
147
148

To estimate the heritability attributable to SNPs ('SNP heritability'), we calculated the proportion of trait variance explained by the additive effects of 523,028 SNPs. In general, heritability estimates were larger for physiological traits than for behavioral traits (Fig. 3b, Supplementary Table 2), which is consistent with findings in other rodent GWAS¹⁷⁻¹⁹. Mean heritability was 0.355 (se=0.045) for physiological traits and 0.168 (se=0.038) for behavioral traits (conditioned place preference, locomotor sensitization, and habituation to startle were not found to have a genetic component and were excluded from the mean). In general, traits with higher heritabilities yielded more associations (Supplementary Fig. 2). However, there was no significant relationship between heritability and effect size at individual loci (Supplementary Fig. 3), suggesting that high heritability does not reliably predict the presence of large-effect alleles.



149
150
151
152
153
154
155
156
157

Figure 3. Manhattan plot and heritability for 120 traits measured in the LG x SM AIL. We identified 126 loci for behavioral and physiological traits using 1,063 mice from G50-56 of the LG x SM AIL. A Manhattan plot of GWAS results is shown in (a). Associations for related traits are grouped by color. For clarity, related traits that mapped to the same locus (Supplementary Table S1) are highlighted only once. The dashed line indicates a permutation-derived significance threshold of $-\log_{10}(p)=5.09$ ($p=8.06 \times 10^{-6}$; $\alpha=0.05$). (b) For a representative subset of traits, SNP heritability estimates (percent trait variance explained by 523,028 GWAS SNPs) for a subset of traits are shown. Precise estimates of heritability with standard error are provided for all traits in Supplementary Table 2.

158

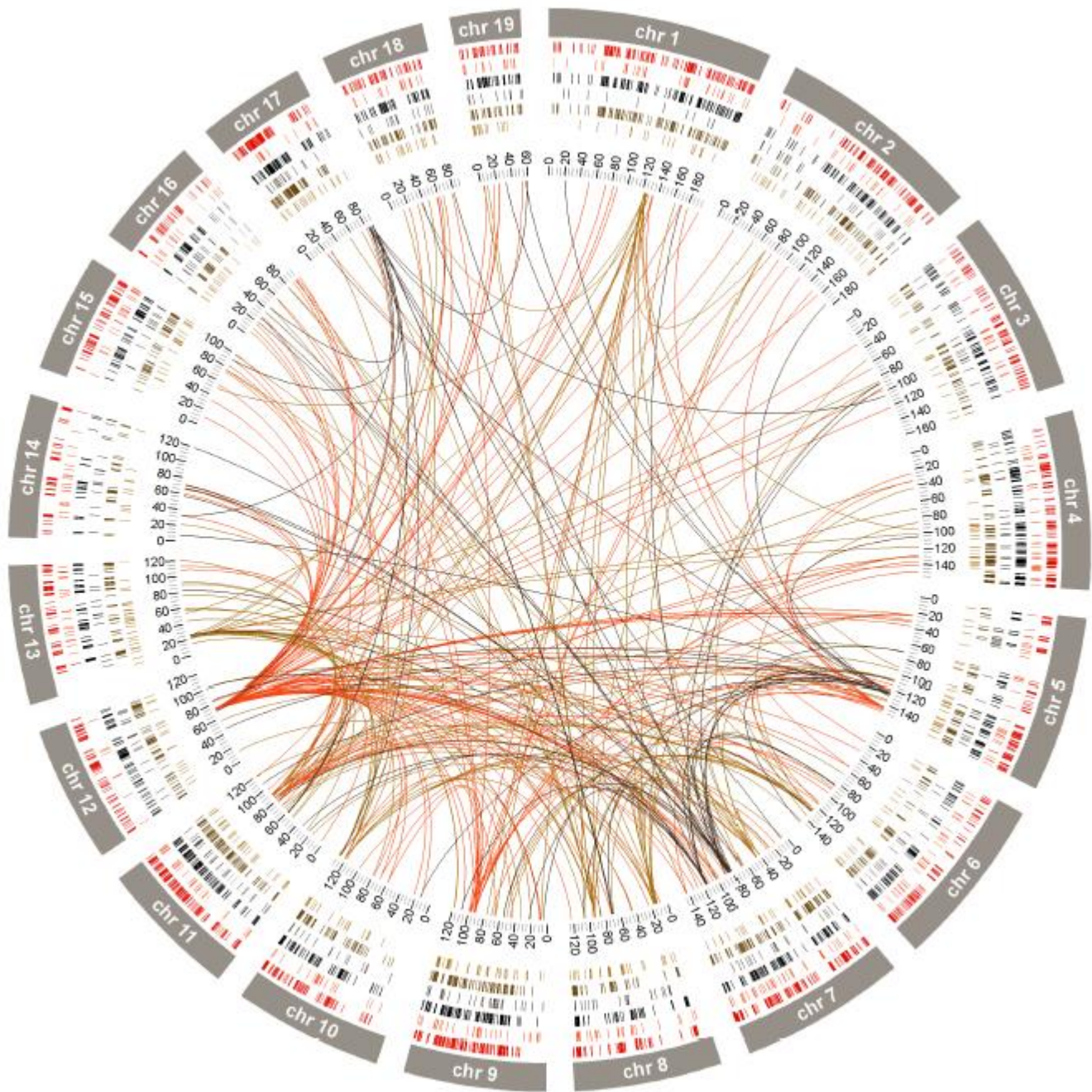
eQTLs

159
160
161

For a subset of phenotyped and genotyped mice, we used RNA-sequencing (RNA-seq) to measure gene expression in the hippocampus (HIP), prefrontal cortex (PFC) and striatum (STR) ($\alpha=0.05$; Fig. 4, Supplementary Fig. 4). We identified 2,902 *cis*-eQTLs in HIP, 2,125 *cis*-eQTLs in PFC and 2,054 *cis*-eQTLs in STR; 1,087 *cis*-eQTLs were

162 significant in all three tissues (FDR<0.05; **Supplementary Table 3**). We also identified 562 HIP *trans*-eQTLs, 408 PFC
163 *trans*-eQTLs and 506 STR *trans*-eQTLs ($p<0.05$; **Supplementary Fig. 5; Supplementary Table 4**).

164
165 Previous studies in model organisms have identified *trans*-eQTLs that regulate the expression of many genes^{4,20,21}; we
166 refer to these as '**master eQTLs**'. We identified several master eQTLs, including one on chromosome 12 (70.19-73.72
167 Mb) that was associated with the expression of 85 genes distributed throughout the genome (**Fig. 4; Supplementary**
168 **Table 4**). This locus was present in HIP, but not in PFC or STR.



170
171
172 **Figure 4. eQTLs in hippocampus (HIP), prefrontal cortex (PFC) and striatum (STR).** We identified over 7,000 *cis*-eQTLs (FDR
173 < 0.05) and over 1,400 *trans*-eQTLs ($\alpha=0.05$) in HIP (n=208; outer red for *cis*-eQTLs, inner red for *trans*-eQTLs), PFC (n=185; outer
174 black for *cis*-eQTLs, inner black for *trans*-eQTL) and STR (n=169; outer brown for *cis*-eQTLs, inner brown for *trans*-eQTLs). We
175 also identified master eQTLs, which we defined as loci that regulate the expression of ten or more target eGenes in a given tissue
176 (central lines link master eQTLs to eGenes).

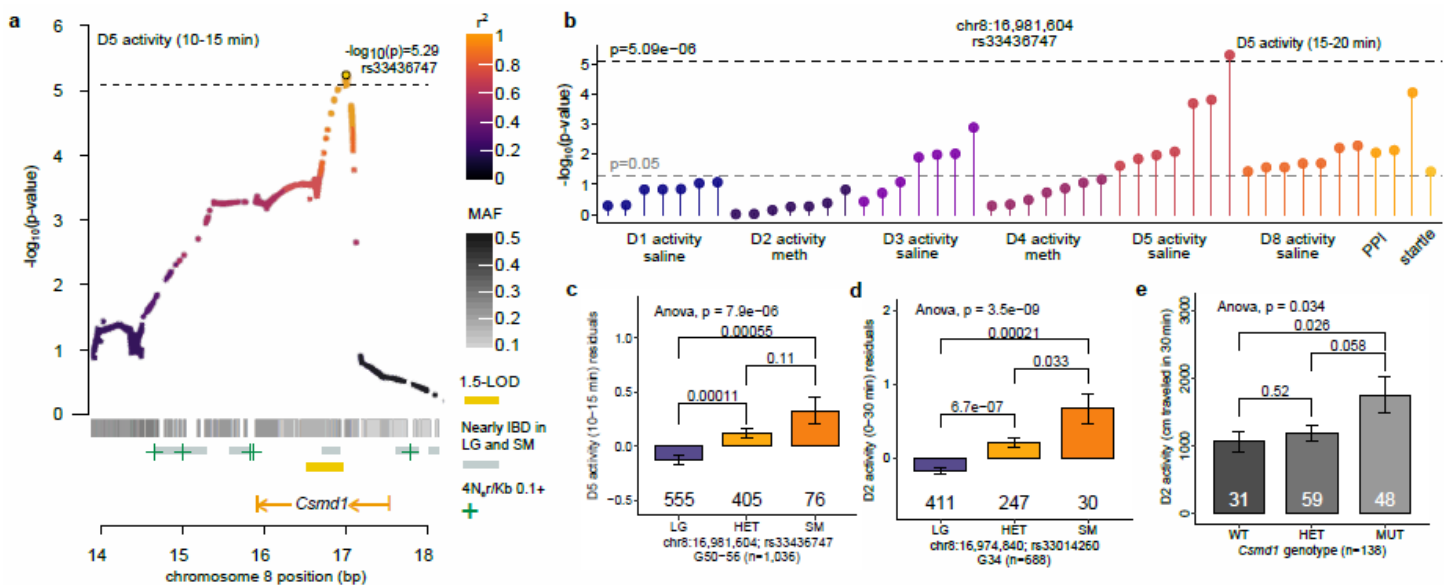
177 Integration of eQTLs and behavioral GWAS results

178 Based on results from human GWAS^{3,4}, we hypothesized that most loci associated with behavior were due to gene
 179 expression differences. For example, four loci associated with locomotor behavior mapped to the same region on
 180 chromosome 17 (**Supplementary Table 1; Supplementary Fig. 2**). The narrowest of these (D1 side changes, 15-20
 181 min; $p=3.60 \times 10^{-6}$) identified a locus that contains a single gene, *Crim1* (cysteine rich transmembrane BMP regulator 1),
 182 which had a significant *cis*-eQTL in HIP. It would be tempting to conclude that *Crim1* is the best candidate to explain
 183 the associations with locomotor behavior; however, two nearby genes, *Qpct* (glutamyl-peptide cyclotransferase) and
 184 *Vit* (vitrin), though physically located outside of the locus, also had *cis*-eQTLs within the locomotor-associated region
 185 (**Supplementary Table 3**). We therefore consider all three genes valid candidates to explain the association with
 186 locomotor behavior.

188 One of the most significant loci we identified was an association with the startle response, also on chromosome 17
 189 ($p=5.28 \times 10^{-10}$; **Fig. 3; Supplementary Fig. 2**). This result replicated a previous association with startle from a prior
 190 study using G34 mice⁸. We performed a phenome-wide association analysis (**PheWAS**) which showed that this region
 191 pleiotropically affected multiple other traits, including locomotor activity following saline and methamphetamine
 192 administration (**Supplementary Fig. 6**). This region was also implicated in conditioned fear and anxiety in our prior
 193 studies of G34 mice⁹, demonstrating that it has extensive pleiotropic effects on behavior. Because the association with
 194 startle identifies a relatively large haplotype that includes over 25 eGenes, our data cannot clarify whether the
 195 pleiotropic effects are due to one or several genes in this interval.

197 We also identified a 0.49-Mb locus on chromosome 8 that was associated with locomotor activity (**Fig. 5a;**
 198 **Supplementary Table 1**); this region was nominally associated with PPI and multiple other activity traits (**Fig. 5b**). The
 199 region identified in the present study (**Fig. 5a-c**) replicates a finding from our previous study using G34 mice⁷ (**Fig. 5d**).
 200 In both cases, the SM allele conferred increased activity (**Fig. 5c,d**) and the implicated locus contained only one gene:
 201 *Csmd1* (CUB and sushi multiple domains 1; **Fig. 5b; Supplementary Table 2**); furthermore, the only *cis*-eQTL that
 202 mapped to this region was for *Csmd1* (**Supplementary Fig. 7**). We obtained mice in which the first exon of *Csmd1*
 203 was deleted to test the hypothesis that *Csmd1* is the QTG for this locus. *Csmd1* mutant mice exhibited increased
 204 activity compared to heterozygous and wild-type mice (**Fig. 5e**), similar to the SM allele. This result is consistent with
 205 the hypothesis that *Csmd1* is the causal gene.

206



207

208

209 **Figure 5. Replication of an association between *Csmd1* and locomotor activity.** (a) Regional plot drawn from all 4.3M SNPs
 210 showing the association between rs33436747 and D5 activity levels. The location of *Csmd1*, 1.5-LOD interval (gold bar), areas of
 211 elevated recombination from Brunshwig et al. (ref. 22) (green plus symbols), regions predicted by Nikolskiy et al. (ref. 13) to be
 212 nearly IBD between LG and SM (grey bars), and SNP MAFs (grey heatmap) are indicated. Points are colored by LD (r^2) with
 213 rs33436747. The dashed line indicates a significance threshold of $-\log_{10}(p) = 5.09$ ($\alpha = 0.05$). (b) PheWAS plot of associations
 214 between rs33436747 and other behavioral traits measured in G50-56 mice. (c) Bar plot of quantile-normalized residuals of
 215 locomotor activity at the *Csmd1* locus are plotted for G50-56 mice. (d) Bar plot of quantile-normalized residuals of locomotor activity
 216 at the *Csmd1* locus for G34 mice from Cheng et al. (ref. 7). rs33436747 was not genotyped in G34; therefore, we plotted activity by
 217 genotype at the nearest SNP (rs33014260; 6,764 bp upstream of rs33436747). (e) Bar plot of locomotor activity data (distance

218 traveled in 0-30 min) for *Csmd1* mutant mice. In panels **c-e** the number of mice in each genotype class is shown below the
219 corresponding bar. ANOVA and two-sided t-test (95% confidence level) p-values are shown for each comparison.

220
221 We identified seven overlapping loci for locomotor activity on chromosome 4 (**Supplementary Table 1;**
222 **Supplementary Fig. 2**). The strongest locus (D5 activity, 0-30 min; $p=6.75 \times 10^{-9}$) spanned 2.31 Mb and completely
223 encompassed the narrowest locus, which spanned 0.74 Mb (D5 activity, 25-30 min; $p=4.66 \times 10^{-8}$); therefore, we
224 focused on the smaller region. *Oprd1* (opioid receptor delta-1) was a *cis*-eGene in all three brain regions; the SM allele
225 conferred an increase in locomotor activity and was associated with decreased expression of *Oprd1*. *Oprd1* knockout
226 mice have been reported to display increased activity relative to wild-type mice²³, suggesting that differential
227 expression of *Oprd1* could explain the locomotor effect at this locus. However, the presence of other genes and
228 eGenes within the region make it difficult to determine whether *Oprd1* is the only QTG.

229
230 We identified an association with D1 locomotor behavior on chromosome 6 at rs108610974, which is located in an
231 intron of *Itpr1* (inositol 1,4,5-trisphosphate receptor type 1; **Supplementary Fig. 8**). This locus contained three *cis*-
232 eGenes and seven *trans*-eQTLs (**Supplementary Fig. 8**). One of the *trans*-eGenes targeted by the locus (*Capn5*;
233 calpain 5) was most strongly associated with rs108610974 and may be the QTG (**Supplementary Table 4**). These
234 results illustrate how the knowledge of both *cis*- and *trans*-eQTLs informed our search for QTGs.

235 Pleiotropic effects on physiological traits

236 Because LG and SM were created by selective breeding for large (LG) and small (SM) body size, this AIL is expected
237 to segregate numerous body size alleles^{11,24}. We measured body weight at ten timepoints throughout development and
238 identified 46 associations. There was extensive pleiotropy among body weight, muscle mass, and bone length
239 (**Supplementary Table 1; Supplementary Fig. 9-12**). Accounting for pleiotropic genetic architecture, eight major loci
240 arose that influenced body weight at multiple timepoints (**Fig. 3a; Supplementary Table 1**).

241
242 For example, eight body weight timepoints mapped to a region on chromosome 2, where the LG allele was associated
243 with smaller body mass (**Supplementary Table 1; Supplementary Fig. 2,9**). The narrowest region spanned 0.08 Mb
244 and did not contain any genes. However, the 0.08-Mb interval contained a *cis*-eQTL SNP for *Nr4a2* (nuclear receptor
245 subfamily 4, group A, member 2) in PFC. Mice lacking *Nr4a2* in midbrain dopamine neurons exhibit a 40% reduction in
246 body weight²⁵. Consistent with this, the LG allele was associated with decreased expression of *Nr4a2*.

247
248 All body weight timepoints were associated with a locus on chromosome 7 (**Supplementary Table 1; Supplementary**
249 **Fig. 2**). We also identified associations for tibialis anterior (TA), gastrocnemius, plantaris weight that partially
250 overlapped this region (**Supplementary Fig. 10**). Although the most significant SNP associated with muscle weight
251 was ~5 Mb downstream of the top body weight SNP, the LG allele was associated with greater weight at both loci
252 (**Supplementary Table 1**). For eight out of ten body weight timepoints, the most significant association fell within *Tpp1*
253 (tripeptidyl peptidase 1), which was a *cis*-eGene in all tissues and a *trans*-eGene targeted by the master HIP eQTL on
254 chromosome 12 (**Fig. 4**). To our knowledge, *Tpp1* has not been shown to affect body size in mice or humans;
255 however, four other *cis*-eGenes in the region have been associated with human body mass index (*Rpl27a*, *Stk33*,
256 *Trim66*, and *Tub*)^{26,27}. Dysfunction of *Tub* (tubby bipartite transcription factor) causes late-onset obesity in mice,
257 perhaps due to *Tub*'s role in insulin signaling²⁸. In addition, several *trans*-eGenes map to this interval, including *Gnb1*
258 (G protein subunit beta 1), which forms a complex with *Tub*²⁹. Another *trans*-eGene associated with this interval,
259 *Crebbp* (CREB binding protein), has been associated with juvenile obesity in human GWAS³⁰.

260 Multiple strong associations identified for muscle mass

261 We examined five hind limb muscle traits, identifying 22 loci (**Supplementary Table 1; Supplementary Fig. 2**). No
262 loci were identified for soleus weight. The strongest association we identified in this study was for extensor digitorum
263 longus (EDL) weight ($p=2.03 \times 10^{-13}$; **Supplementary Table 1; Supplementary Fig. 11**). An association with
264 gastrocnemius weight provided additional support for the region ($p=2.56 \times 10^{-7}$; **Supplementary Fig. 11**); in both cases,
265 the SM allele was associated with increased muscle mass. Each locus spans less than 0.5 Mb and is flanked by
266 regions of low polymorphism between LG and SM (**Supplementary Fig. 11, Supplementary Table 1**). Two *cis*-
267 eGenes within the region, *Trappc13* (trafficking protein particle complex 13) and *Nln* (neurolysin), are differentially
268 expressed in LG and SM soleus³¹ and TA³², with LG exhibiting increased expression of both genes. While there is no
269 known relationship between *Trappc13* and muscle, *Nln* has been shown to play a role in mouse skeletal muscle³³.

270
271 The LG allele was associated with greater EDL, plantaris, and TA weight at another locus on chromosome 4
272 (**Supplementary Table 1; Supplementary Fig. 12**). The loci for EDL and plantaris spanned ~0.5 Mb, defining a region

273 that contained six genes (**Supplementary Table 1**). The top SNPs for EDL (rs239008301; $p=7.88 \times 10^{-13}$) and plantaris
274 (rs246489756; $p=2.25 \times 10^{-6}$) were located in an intron of *Astn2* (astrotactin 2), which is differentially expressed in LG
275 and SM soleus³¹. SM, which exhibits lower expression of *Astn2* in soleus relative to LG³¹, has a 16 bp insertion in an
276 enhancer region 6.6 kb upstream of *Astn2* (ENSMUSR00000192783)¹³. Two other genes in this region have been
277 associated with muscle or bone phenotypes traits in the mouse: *Tlr4* (toll-like receptor 4), which harbors one
278 synonymous coding mutation on the SM background (rs13489095) and *Trim32* (tripartite motif-containing 32), which
279 contains no coding polymorphisms between the LG and SM strains.

280 Discussion

281
282 Crosses among well-characterized inbred strains are a mainstay of model organism genetics. In the present study, we
283 used 1,063 male and female mice from LG x SM G50-56 to identify 126 loci for a variety of traits selected for their
284 relevance to human psychiatric and metabolic diseases^{24,34,35} (**Fig. 3; Supplementary Table 1; Supplementary Fig.**
285 **2**). Whereas our previous work established AILs as an effective tool for fine-mapping loci identified in F2 crosses⁷⁻
286 ^{11,14,31}, this study demonstrates that AILs are also a powerful fine mapping population in their own right. We show that
287 several QTGs we identified are corroborated by extant human and mouse genetic data. We also replicated a number
288 of our earlier findings.

289
290 Classical crosses like F₂ and recombinant inbred strains provide poor mapping resolution because the ancestral
291 chromosomes persist as extremely long haplotypes². To address this limitation, we and others have used AILs¹⁴.
292 Because both inbred strains contribute equally to an AIL, there are numerous common variants (**Fig. 1a,b**), and each
293 successive generation further degrades LD between adjacent SNPs (**Fig. 1c**). In addition to AILs, a number of other
294 outbred populations have been used in rodent GWAS, including CFW mice^{17,18}, Diversity Outbred (**DO**) mice^{36,37}, and
295 N/NIH heterogeneous stock rats (**HS**)^{19,38}. CFW mice are obtained from a commercial vendor, which avoids the
296 expenses of maintaining a colony. In addition, non-siblings can be obtained, which reduces the complicating effects
297 that can occur when close relatives are used in GWAS. However, the CFW founder strains are unavailable, and many
298 alleles exist at low frequencies among CFWs, limiting power and introducing genetic noise^{17,18}. Commercially available
299 DO mice are more expensive than CFWs, but like AILs, the founder strains have been fully sequenced, which allows
300 imputation of SNPs and founder haplotypes. However, three of the eight inbred strains used to produce the DO are so-
301 called wild-derived strains; making DO mice very difficult to handle, which complicates many behavioral procedures³⁷.
302 Furthermore, the causal alleles in the DO are often from one of the wild derived strains, because 8 strains contributed
303 equally to the DO, this means that the causal allele frequencies are often in the range of 0.125. Finally, N/NIH HS rats,
304 which are conceptually very similar to DO mice, have also been used as a fine mapping population^{19,38}. Among these
305 options, AILs stand out for their simplicity, balanced allele frequency and ease of handling.

306
307 A major goal of this study was to identify the genes that are responsible for the loci implicated in behavioral and
308 physiological traits. The mapping resolution of the LG x SM AIL was critically important for this goal. However, no
309 matter how precise the resolution, proximity of a gene to the associated SNP is never sufficient to establish causality⁴.
310 Therefore, we used RNA-seq to quantify mRNA abundance in three brain regions that are strongly implicated in the
311 behavioral traits: HIP, PFC and STR. We used these data to identify 7,081 *cis*-eQTLs and 1,372 *trans*-eQTLs (**Fig. 4,**
312 **Supplementary Fig. 4-5; Supplementary Tables 3-4**). In a few cases, loci contained only a single eQTL; however, in
313 most cases multiple *cis*-eQTLs and *trans*-eQTLs mapped to the implicated loci. Thus, we frequently incorporated
314 functional information, including data about tissue specific expression, coding SNP, mutant mice, and human genetic
315 studies to parse among the implicated genes.

316
317 We have previously shown that GBS is a cost-effective strategy for genotyping CFW mice³⁹. The advantages of GBS
318 were even greater for this AIL because imputation allowed us to easily obtain 4.3M SNPs while using only half the
319 sequencing depth (**Fig. 1a**). Even before imputation, GBS yielded nearly 50% more informative SNPs compared to the
320 best available SNP genotyping chip¹² at about half the cost (**Supplementary Fig. 1**).

321
322 One of the goals of this study was to perform GWAS for conditioned place preference (**CPP**), which is a well-validated
323 measure of the reinforcing effects of drugs⁴⁰. Unfortunately, the heritability of CPP in this study was not significantly
324 different from zero (**Fig. 3b**). This result was partially consistent with our prior study in which we used a higher dose of
325 methamphetamine (2 vs. the 1 mg/kg used in the present study)⁴¹. The low heritability of CPP in this AIL likely reflects
326 a lack of relevant genetic variation in this specific population since both panels of inbred strains and genetically
327 engineered mutant alleles show differences in CPP^{40,42,43}, demonstrating the existence of heritable variance in other
328 populations. It is possible that even lower doses of methamphetamine, which might fall on the ascending portion of the
329 dose-response function, would have resulted in higher heritability. Similarly, responses to other drugs or different CPP
330 methodology may have exhibited greater heritability.

331

332

333

334

335

336

337

338

339

340

341

342

343

344

345

346

347

348

349

350

351

352

353

354

355

We used PheWAS to identify pleiotropic effects of several loci identified in this study. In many cases, pleiotropy involved highly correlated traits such as body weight on different days or behavior at different time points within a single day (**Supplementary Fig. 9-13; Supplementary Table 1**). We also observed more surprising examples of pleiotropy, including pleiotropy between locomotor activity and gastrocnemius mass on chromosome 4 (**Supplementary Fig. 14**), and pleiotropy between locomotor activity and the startle response on chromosome 12 (**Supplementary Fig. 15**). We also observed extensive pleiotropy on chromosome 17; this locus influenced saline- and methamphetamine-induced locomotor activity and startle response (**Supplementary Fig. 6**). Moreover, this same region had been previously implicated in anxiety-like behavior⁹, contextual and conditioned fear⁹, and startle response⁸ in prior studies of LG x SM G34, suggesting that the locus has a broad impact on many behavioral traits. These results support the idea that pleiotropy is a pervasive feature in this AIL and provide further evidence of the replicability of the loci identified by this and prior GWAS.

Discoveries from human GWAS are often considered preliminary until they are replicated in an independent cohort. In model organisms, replication using an independent cohort is rarely employed because it is possible to directly manipulate the implicated gene. We replicated one behavioral locus identified in this study using the criteria of both human and model organism genetics. We had previously identified an association with locomotor activity on chromosome 8 using G34 of this AIL⁷, which was replicated in the present study (**Fig. 5**). In both cases, the SM allele was associated with lower activity (**Fig. 5c-d**). We also identified a locus for PPI (76 dB) in this region (**Fig. 5a; Supplementary Table 1, Supplementary Fig. 2**). The loci identified in both G34 and in G50-56 were small and contained just one gene: *Csmd1* (**Fig. 5b**). In the present study we also identified a *cis*-eQTL for *Csmd1* in HIP (**Supplementary Figure 7**). Finally, we obtained *Csmd1* mutant mice⁴⁴ and found that they also showed altered locomotor activity (**Fig. 5e**). Thus, we have demonstrated replication both by performing an independent GWAS and by performing an experimental manipulation that recapitulates the phenotype.

356

Online Methods

357

Genetic background

358

359

360

361

362

363

364

365

366

367

368

The LG and SM inbred strains were independently selected for high and low body weight at 60 days⁴⁵. The LG x SM AIL was derived from an F₁ intercross of SM females and LG males initiated by Dr. James Cheverud at Washington University in St. Louis⁶. Subsequent AIL generations were maintained using at least 65 breeder pairs selected by pseudo-random mating⁴⁶. In 2006, we established an independent AIL colony using 140 G33 mice obtained from Dr. Cheverud (Jmc: LG,SM-G33). Since 2009, we have selected breeders using an R script (**Supplementary Note**) that leverages pairwise kinship coefficients estimated from the AIL pedigree to select the most unrelated pairs while also attempting to minimize mean kinship among individuals in the incipient generation (the full pedigree is included in **Supplementary File 1**). We maintained ~100 breeder pairs in G49-55 to produce the mice for this study. In each generation, we used one male and one female from each nuclear family for phenotyping, and reserved up to three of their siblings for breeding the next generation.

369

Phenotypes

370

371

372

373

374

375

376

377

378

379

380

381

382

We subjected 1,123 AIL mice (562 female, 561 male; Aap: LG,SM-G50-56) to a four-week battery of tests over the course of two years. This sample size was based on an analysis suggesting that 1,000 mice would provide 80% power to detect associations explaining 3% of the phenotypic variance (**Supplementary Fig. 16**). We measured CPP for 1 mg/kg methamphetamine, locomotor behavior, PPI, startle, body weight, muscle mass, bone length and other related traits (**Supplementary Table 2**). We tested mice during the light phase of a 12:12h light-dark cycle in 22 batches comprised of 24-71 individuals (median=53.5). Median age was 54 days (mean=55.09, range=35-101) at the start of testing and 83 days (mean=84.4, range=64-129) at death. Standard lab chow and water were available *ad libitum*, except during testing. Testing was performed during the light phase, starting one hour after lights on and ending one hour before lights off. No environmental enrichment was provided. All procedures were approved by the Institutional Animal Care and Use Committee at the University of Chicago (**Supplementary File 2**). Traits are summarized briefly below; detailed descriptions are provided in the **Supplementary Note**.

383

384

385

386

387

388

389

390

391

392

393

394

CPP and locomotor behavior: CPP is an associative learning paradigm that has been used to measure the motivational properties of drugs in humans⁴⁷ and rodents⁴⁰. We defined CPP as the number of seconds spent in a drug-associated environment relative to a neutral environment over the course of 30 minutes. The full procedure takes eight days, which we refer to as **D1-D8**. We measured baseline preference after administration of vehicle (0.9% saline, i.p.) on D1. On D2 and D4, mice were administered methamphetamine (1 mg/kg, i.p.) and restricted to one visually and tactically distinct environment; on D3 and D5 mice were administered vehicle and restricted to the other, contrasting environment. On D8, mice were allowed to choose between the two environments after administration of vehicle; we measured CPP at this time. Other variables measured during the CPP test include the distance traveled (cm) on all testing days, the number of side changes on D1 and D8, and locomotor sensitization to methamphetamine (the increase in activity on D4 relative to D2). We measured CPP and locomotor traits across six 5-minute intervals and summed them to generate a total phenotype for each day.

395

396

397

398

399

400

401

402

PPI and startle: PPI is the reduction of the acoustic startle response when a loud noise is immediately preceded by a low decibel (**dB**) prepulse⁴⁸. PPI and startle are measured across multiple trials that occur over four consecutive blocks of time⁸. The primary startle trait is the mean startle amplitude across all pulse-alone trials in blocks 1-4. Habituation to startle is the difference between the mean startle response at the start of the test (block 1) and the end of the test (block 4). PPI, which we measured at three prepulse intensities (3, 6, and 12 dB above 70 dB background noise), is the mean startle response during pulse-alone trials in blocks 2-3 normalized by the mean startle response during prepulse trials in blocks 2-3.

403

404

405

406

407

408

409

Physiological traits: We measured body weight (g) on each testing day and at the time of death. One week after PPI, we measured blood glucose levels (mg/dL) after a four-hour fast. One week after glucose testing, we killed the mice, and measured tail length (cm from base to tip of the tail). We stored spleens in a 1.5 mL solution of 0.9% saline at -80°C until DNA extraction. We removed the left hind limb of each mouse just below the pelvis; hind limbs were stored at -80°C. Frozen hind limbs were phenotyped by Dr. Arimantas Lionikas at the University of Aberdeen. Phenotyped muscles include two dorsiflexors, TA and EDL, and three plantar flexors: gastrocnemius, plantaris and soleus. We isolated individual muscles under a dissection microscope and weighed them to 0.1 mg precision on a Pioneer balance

410 (Ohaus, Parsippany, NJ, USA). After removing soft tissue from the length of tibia, we measured its length to 0.01 mm
411 precision with a Z22855 digital caliper (OWIM GmbH & Co., Neckarsulm, GER).
412

413 **Brain tissue:** We collected HIP, PFC and STR for RNA-seq from the brain of one mouse per cage. This allowed us to
414 dissect each brain within five minutes of removing a cage from the colony room (rapid tissue collection was intended to
415 limit stress-induced changes in gene expression). We preselected brain donors to prevent biased sampling of docile
416 (easily caught) mice and to avoid sampling full siblings, which would reduce our power to detect eQTLs. Intact brains
417 were extracted and submerged in chilled RNALater (Ambion, Carlsbad, CA, USA) for one minute before dissection.
418 Individual tissues were stored separately in chilled 0.5-mL tubes of RNALater. All brain tissue was dissected by the
419 same experimenter and subsequently stored at -80°C until extraction.

420 GBS variant calling and imputation

421
422 GBS is a reduced-representation genotyping method^{49,50} that we have adapted for use in mice and rats^{17,39}. We
423 extracted DNA from spleen using a standard salting-out protocol and prepared GBS libraries by digesting DNA with the
424 restriction enzyme *Pst*I, as described previously¹⁷. We sequenced 24 uniquely barcoded samples per lane of an
425 Illumina HiSeq 2500 using single-end, 100 bp reads. We aligned 1,110 GBS libraries to the mm10 reference genome
426 before using GATK⁵¹ to realign reads around known indels in LG and SM¹³ (see **Supplementary Note** and
427 **Supplementary File 3** for details and example commands). We obtained an average of 3.2M reads per sample. We
428 discarded 32 samples with <1M reads aligned to the main chromosome contigs (1-19, X, Y) or with a primary
429 alignment rate <77% (i.e. three s.d. below the mean of 97.4%; **Supplementary Fig. 17**).
430

431 We used ANGSD⁵² to obtain genotype likelihoods for the remaining 1,078 mice and used Beagle⁵³ for variant calling,
432 which we performed in two stages. We used first-pass variant calls as input for IBDLD^{54,55}, which we used to estimate
433 kinship coefficients for the mice in our sample. Because our sample contained opposite-sex siblings, we were able to
434 identify and resolve sample mix-ups by comparing genetic kinship estimates to kinship estimated from the LG x SM
435 pedigree (described in the **Supplementary Note**). In addition, we re-genotyped 24 mice on the GigaMUGA¹² to
436 evaluate GBS variant calls (**Supplementary Table 5** lists concordance rates at various stages of our pipeline; see
437 **Supplementary Note** for details).
438

439 After identifying and correcting sample mix-ups, we discarded 15 samples whose identities could not be resolved
440 (**Supplementary Note**). Next, we used Beagle^{53,56}, in conjunction with LG and SM haplotypes obtained from whole-
441 genome sequencing data¹³ to impute 4.3M additional SNPs into the final sample of 1,063 mice. We removed SNPs
442 with low MAFs (<0.1), SNPs with Hardy-Weinberg Equilibrium (**HWE**) violations ($p \leq 7.62 \times 10^{-6}$, determined from gene
443 dropping simulations as described in the **Supplementary Note**), and SNPs with low imputation quality (dosage r^2 ,
444 $DR^2 < 0.9$). We then pruned variants in high LD ($r^2 > 0.95$) to obtain the 523,028 SNPs that we used for GWAS.
445

446 LD decay

447
448 We used PLINK⁵⁷ to calculate r^2 for all pairs of autosomal GWAS SNPs typed in G50-56 (parameters are listed in
449 **Supplementary File 3**). We repeated the procedure for 3,054 SNPs that were genotyped in G34 mice⁷. Next, we
450 randomly sampled r^2 values calculated for ~40,000 SNP pairs from each population and used the data to visualize the
451 rate of LD decay (**Fig. 1c**).

452 LOCO-LMM

453
454 We used a modified LMM implemented in GEMMA⁵⁸ to perform GWAS. An LMM accounts for relatedness by modeling
455 the covariance between phenotypes and genotypes as a random, polygenic effect¹⁴, which we also refer to as a
456 genetic relationship matrix (**GRM**). Power to detect associations is reduced when the locus being tested is also
457 included in the GRM because the effect of the locus is represented in both the fixed and random terms¹⁵. To address
458 this issue, we calculated 19 separate GRMs, each one excluding a different chromosome. When testing SNPs on a
459 given chromosome, we used the GRM that did not include markers from that chromosome as the polygenic effect in
460 the model. Fixed covariates for each trait are listed in **Supplementary Table 2**.
461

462 We used a permutation-based approach implemented in MultiTrans⁵⁹ and SLIDE⁶⁰ to obtain a genome-wide
463 significance threshold that accounts for LD between nearby markers (see **Supplementary Note** for details). We
464 obtained a significance threshold of $p = 8.06 \times 10^{-6}$ ($\alpha = 0.05$) from 2.5M samplings. Because the phenotypic data were

465 quantile-normalized, we applied the same threshold to all traits. We converted p-values to LOD scores and used a 1.5-
466 LOD support interval to approximate a critical region around each associated region, which enabled us to
467 systematically identify overlap with eQTLs.

468
469 We estimated the proportion of phenotypic variance explained by the set of 523,028 LD-pruned SNPs using the
470 restricted maximum likelihood algorithm in GEMMA⁵⁸. We ran a second genome-wide scan for each trait, this time
471 dropping the fixed effect of dosage and including the complete GRM estimated from SNPs on all 19 autosomes. We
472 repeated the procedure using dosage at the most significant SNP as a covariate for each trait and interpreted the
473 difference between the two estimates as the effect size of that locus.

474 RNA-sequencing and quality control

475 We extracted mRNA from HIP, PFC and STR as described in Parker *et al.* (ref. 17) and prepared cDNA libraries from
476 741 samples with RNA integrity scores ≥ 8.0 (265 HIP; 240 PFC; 236 STR)⁶¹ as measured on a Bioanalyzer (Agilent,
477 Wilmington, DE, USA). We used Quant-iT kits to quantify RNA (Ribogreen) and cDNA (Picogreen; Fisher Scientific,
478 Pittsburgh, PA, USA). Barcoded sequencing libraries were prepared with the TruSeq RNA Kit (Illumina, San Diego,
479 USA), pooled in sets of 24, and sequenced on two lanes of an Illumina HiSeq 2500 using 100 bp, single-end reads.

480
481 Because mapping quality tends to be higher for reads that closely match the reference genome⁶², read mapping in an
482 AIL may be biased toward the reference strain (C57BL/6J)⁶³. We addressed this concern by aligning RNA-seq reads to
483 custom genomes created from LG and SM using whole-genome sequence data¹³. We used default parameters in
484 HISAT⁶⁴ for alignment and GenomicAlignments⁶⁵ for assembly, assigning each read to a gene as defined by Ensembl
485 (*Mus_musculus*.GRCm38.85)⁶⁶. We required that each read overlap one unique disjoint region of the gene. If a read
486 contained a region overlapping multiple genes, genes were split into disjoint intervals, and any shared regions between
487 them were hidden. If the read overlapped one of the remaining intervals, it was assigned to the gene that the interval
488 originated from; otherwise, it was discarded. Next, we reassigned the mapping position and CIGAR strings for each
489 read to match mm10 genome coordinates and combined the LG and SM alignment files for each sample by choosing
490 the best mapping. Only uniquely mapped reads were included in the final alignment files. We then used DESeq⁶⁷ to
491 obtain normalized read counts for each gene in HIP, PFC and STR. We excluded genes detected in <95% of samples
492 within each tissue.

493
494 We also excluded 30 samples with <5M mapped reads or with an alignment rate <91.48% (i.e. less than 1 s.d. below
495 the mean number of reads or the mean alignment rate across all samples and tissues; **Supplementary Fig. 18**). We
496 merged expression data from HIP, PFC and STR and plotted the first two principal components (**PCs**) of the data to
497 identify potential tissue swaps. Most samples clustered into distinct groups based on tissue. We reassigned 12
498 mismatched samples to new tissues and removed 35 apparently contaminated samples that did not cluster with the
499 rest of the data (**Supplementary Fig. 19**). We also used agreement among GBS genotypes and genotypes called
500 from RNA-seq data in the same individuals to identify and resolve mixed-up samples, as detailed in the
501 **Supplementary Note**. We discarded 108 sample mix-ups that we were not able to resolve, 29 samples with low-
502 quality GBS data, and 12 outliers (details are provided in the **Supplementary Note**). A total of 208 HIP, 185 PFC, and
503 169 STR samples were retained for further analyses.

504
505 Prior to eQTL mapping, we quantile-normalized gene expression data and used principal components analysis to
506 remove the effects of unknown confounding variables⁶⁸. For each tissue, we calculated the first 100 PCs of the gene \times
507 sample gene expression matrix. We quantile-normalized PCs and used GEMMA⁵⁸ to test for association with SNPs
508 using sex and batch as covariates. We evaluated significance with the same permutation-based threshold used for
509 GWAS. We retained PCs that showed evidence of association with a SNP in order to avoid removing *trans*-eQTL
510 effects. We then used linear regression to remove the effects of the remaining PCs (71 in HIP, 81 in STR and 93 in
511 PFC) and quantile-normalized the residuals.

512 eQTL mapping

513 We mapped *cis*- and *trans*-eQTLs using a LOCO-LMM¹⁵ implemented in GEMMA⁵⁸, conservatively including sex and
514 batch as covariates even though PC regression might have accounted for them (see **Supplementary Note** for details).

515
516 We considered intergenic SNPs and SNPs 1 Mb upstream or downstream of the gene as potential *cis*-eQTLs and
517 excluded 2,143 genes that had no SNPs within their *cis*-regions. We used eigenMT⁶⁹ to obtain a gene-based p-value
518 adjusted for the number of independent SNPs in each *cis* region. We declared *cis*-eQTLs significant at an FDR<0.05.
519 We refer to genes with significant *cis*-eQTLs as ***cis*-eGenes**.

520

521 SNPs on chromosomes that did not contain the gene being tested were considered potential *trans*-eQTLs. We
522 determined significance thresholds for *trans*-eQTLs by permuting data 1,000 times. Since expression data were
523 quantile-normalized, we permuted one randomly chosen gene per tissue. The significance threshold for *trans*-eQTLs
524 was 8.68×10^{-6} in STR, 9.01×10^{-6} in in PFC ($\alpha=0.05$). We used all SNPs for permutation; therefore, we expect these
525 thresholds to be conservative. We refer to genes with *trans*-eQTLs as ***trans*-eGenes**. Finally, we defined *trans*-eQTL
526 hotspots or '**master eQTLs**' as 5 Mb regions that contain ten or more *trans*-eQTLs. To identify master eQTLs, we
527 divided chromosomes into 5 Mb bins and assigned each *trans*-eGene to the bin containing its most significant eQTL
528 SNP.

529 *Csmd1* mutant mice

530 *Csmd1* mutants were created by Lexicon Genetics by inserting a Neomycin cassette into the first exon of *Csmd1* using
531 embryonic stem cells derived from 129S5 mice⁷⁰ as described by Distler *et al.* (ref. ⁴⁴). The mice we used were the
532 result of a C57BL/6 x 129S5 intercross designated B6;129S5-*Csmd1*^{tm1Lex}/Mmucd (the exact C57BL/6 substrain is
533 unknown). We bred heterozygous males and females and tested littermate offspring to account for their mixed genetic
534 background. *Csmd1* spans 1.6 Mb and has 70 exons. Its four major transcripts, termed *Csmd1-1* to *Csmd1-4*, are
535 expressed in the central nervous system⁴⁴. Distler *et al.* (ref. ⁴⁴) demonstrated that *Csmd1* homozygous mutant mice
536 express <30% of wild-type *Csmd1* levels in the brain, and heterozygous mice show a 54% reduction in *Csmd1*
537 expression. Residual expression of *Csmd1* in homozygous mutant mice is derived from *Csmd1-4*, the only transcript
538 that does not include the first exon. We analyzed locomotor behavior on two days following a saline injection in 31
539 wild-type, 59 heterozygous, and 48 mutant mice.
540

541 References

542 Introduction, Results and Discussion

- 543 1. Flint, J. & Mackay, T. F. C. Genetic architecture of quantitative traits in mice, flies, and humans. *Genome Res.* **19**,
- 544 723–733 (2009).
- 545 2. Parker, C. C. & Palmer, A. A. Dark matter: are mice the solution to missing heritability? *Front. Genet.* **2**, 32 (2011).
- 546 3. GTEx Consortium *et al.* Genetic effects on gene expression across human tissues. *Nature* **550**, 204–213 (2017).
- 547 4. Albert, F. W. & Kruglyak, L. The role of regulatory variation in complex traits and disease. *Nat. Rev. Genet.* **16**,
- 548 197–212 (2015).
- 549 5. Darvasi, A. & Soller, M. Advanced intercross lines, an experimental population for fine genetic mapping. *Genetics*
- 550 **141**, 1199–1207 (1995).
- 551 6. Ehrich, T. H. *et al.* Fine-mapping gene-by-diet interactions on chromosome 13 in a LGVJ X SMVJ murine model of
- 552 obesity. *Diabetes* **54**, 1863–1872 (2005).
- 553 7. Cheng, R. *et al.* Genome-wide association studies and the problem of relatedness among advanced intercross
- 554 lines and other highly recombinant populations. *Genetics* **185**, 1033–1044 (2010).
- 555 8. Samocha, K. E., Lim, J. E., Cheng, R., Sokoloff, G. & Palmer, A. A. Fine mapping of QTL for prepulse inhibition in
- 556 LG/J and SM/J mice using F(2) and advanced intercross lines. *Genes Brain Behav.* **9**, 759–767 (2010).
- 557 9. Parker, C. C. *et al.* High-resolution genetic mapping of complex traits from a combined analysis of F2 and
- 558 advanced intercross mice. *Genetics* **198**, 103–116 (2014).
- 559 10. Lionikas, A., Cheng, R., Lim, J. E., Palmer, A. A. & Blizard, D. A. Fine-mapping of muscle weight QTL in LG/J and
- 560 SM/J intercrosses. *Physiol. Genomics* **42A**, 33–38 (2010).
- 561 11. Parker, C. C. *et al.* Fine-mapping alleles for body weight in LG/J X SM/J F2 and F(34) advanced intercross lines.
- 562 *Mamm. Genome Off. J. Int. Mamm. Genome Soc.* **22**, 563–571 (2011).
- 563 12. Morgan, A. P. *et al.* The Mouse Universal Genotyping Array: From Substrains to Subspecies. *G3 Bethesda Md* **6**,
- 564 263–279 (2015).
- 565 13. Nikolskiy, I. *et al.* Using whole-genome sequences of the LG/J and SM/J inbred mouse strains to prioritize
- 566 quantitative trait genes and nucleotides. *BMC Genomics* **16**, 415 (2015).
- 567 14. Gonzales, N. M. & Palmer, A. A. Fine-mapping QTLs in advanced intercross lines and other outbred populations.
- 568 *Mamm. Genome Off. J. Int. Mamm. Genome Soc.* **25**, 271–292 (2014).
- 569 15. Cheng, R., Parker, C. C., Abney, M. & Palmer, A. A. Practical considerations regarding the use of genotype and
- 570 pedigree data to model relatedness in the context of genome-wide association studies. *G3 Bethesda Md* **3**, 1861–
- 571 1867 (2013).
- 572 16. Listgarten, J. *et al.* Improved linear mixed models for genome-wide association studies. *Nat. Methods* **9**, 525–526
- 573 (2012).
- 574 17. Parker, C. C. *et al.* Genome-wide association study of behavioral, physiological and gene expression traits in
- 575 outbred CFW mice. *Nat. Genet.* **48**, 919–926 (2016).
- 576 18. Nicod, J. *et al.* Genome-wide association of multiple complex traits in outbred mice by ultra low-coverage
- 577 sequencing. *Nat. Genet.* **48**, 912–918 (2016).
- 578 19. Rat Genome Sequencing and Mapping Consortium *et al.* Combined sequence-based and genetic mapping
- 579 analysis of complex traits in outbred rats. *Nat. Genet.* **45**, 767–775 (2013).
- 580 20. Chesler, E. J. *et al.* Complex trait analysis of gene expression uncovers polygenic and pleiotropic networks that
- 581 modulate nervous system function. *Nat. Genet.* **37**, 233–242 (2005).
- 582 21. Hasin-Brumshtein, Y. *et al.* Hypothalamic transcriptomes of 99 mouse strains reveal trans eQTL hotspots, splicing
- 583 QTLs and novel non-coding genes. *eLife* **5**, (2016).
- 584 22. Brunschwig, H. *et al.* Fine-scale maps of recombination rates and hotspots in the mouse genome. *Genetics* **191**,
- 585 757–764 (2012).
- 586 23. Filliol, D. *et al.* Mice deficient for delta- and mu-opioid receptors exhibit opposing alterations of emotional
- 587 responses. *Nat. Genet.* **25**, 195–200 (2000).
- 588 24. Lawson, H. A. & Cheverud, J. M. Metabolic syndrome components in murine models. *Endocr. Metab. Immune*
- 589 *Disord. Drug Targets* **10**, 25–40 (2010).
- 590 25. Kadkhodaei, B. *et al.* Nurr1 is required for maintenance of maturing and adult midbrain dopamine neurons. *J.*
- 591 *Neurosci. Off. J. Soc. Neurosci.* **29**, 15923–15932 (2009).
- 592 26. Berndt, S. I. *et al.* Genome-wide meta-analysis identifies 11 new loci for anthropometric traits and provides
- 593 insights into genetic architecture. *Nat. Genet.* **45**, 501–512 (2013).
- 594 27. Locke, A. E. *et al.* Genetic studies of body mass index yield new insights for obesity biology. *Nature* **518**, 197–206
- 595 (2015).
- 596 28. Stretton, C., Litherland, G. J., Moynihan, A., Hajduch, E. & Hundal, H. S. Expression and modulation of TUB by
- 597 insulin and thyroid hormone in primary rat and murine 3T3-L1 adipocytes. *Biochem. Biophys. Res. Commun.* **390**,
- 598 1328–1333 (2009).
- 599 29. Baehr, W. & Frederick, J. M. Naturally occurring animal models with outer retina phenotypes. *Vision Res.* **49**,
- 600 2636–2652 (2009).

- 601 30. Comuzzie, A. G. *et al.* Novel genetic loci identified for the pathophysiology of childhood obesity in the Hispanic
602 population. *PLoS One* **7**, e51954 (2012).
- 603 31. Carroll, A. M. *et al.* Fine-mapping of genes determining extrafusal fiber properties in murine soleus muscle.
604 *Physiol. Genomics* **49**, 141–150 (2017).
- 605 32. Lionikas, A. *et al.* Resolving candidate genes of mouse skeletal muscle QTL via RNA-Seq and expression network
606 analyses. *BMC Genomics* **13**, 592 (2012).
- 607 33. Cavalcanti, D. M. L. P. *et al.* Neurolysin knockout mice generation and initial phenotype characterization. *J. Biol.*
608 *Chem.* **289**, 15426–15440 (2014).
- 609 34. Swerdlow, N. R., Braff, D. L. & Geyer, M. A. Sensorimotor gating of the startle reflex: what we said 25 years ago,
610 what has happened since then, and what comes next. *J. Psychopharmacol. Oxf. Engl.* **30**, 1072–1081 (2016).
- 611 35. de Wit, H. & Phillips, T. J. Do initial responses to drugs predict future use or abuse? *Neurosci. Biobehav. Rev.* **36**,
612 1565–1576 (2012).
- 613 36. Gatti, D. M. *et al.* Quantitative trait locus mapping methods for diversity outbred mice. *G3 Bethesda Md* **4**, 1623–
614 1633 (2014).
- 615 37. Logan, R. W. *et al.* High-precision genetic mapping of behavioral traits in the diversity outbred mouse population.
616 *Genes Brain Behav.* **12**, 424–437 (2013).
- 617 38. Tsaih, S.-W. *et al.* Identification of a novel gene for diabetic traits in rats, mice, and humans. *Genetics* **198**, 17–29
618 (2014).
- 619 39. Fitzpatrick, C. J. *et al.* Variation in the form of Pavlovian conditioned approach behavior among outbred male
620 Sprague-Dawley rats from different vendors and colonies: sign-tracking vs. goal-tracking. *PLoS One* **8**, e75042
621 (2013).
- 622 40. Tzschentke, T. M. Measuring reward with the conditioned place preference (CPP) paradigm: update of the last
623 decade. *Addict. Biol.* **12**, 227–462 (2007).
- 624 41. Bryant, C. D., Kole, L. A., Guido, M. A., Cheng, R. & Palmer, A. A. Methamphetamine-induced conditioned place
625 preference in LG/J and SM/J mouse strains and an F45/F46 advanced intercross line. *Front. Genet.* **3**, 126 (2012).
- 626 42. Philip, V. M. *et al.* High-throughput behavioral phenotyping in the expanded panel of BXD recombinant inbred
627 strains. *Genes Brain Behav.* **9**, 129–159 (2010).
- 628 43. Martinelli, D. C. *et al.* Expression of C1ql3 in Discrete Neuronal Populations Controls Efferent Synapse Numbers
629 and Diverse Behaviors. *Neuron* **91**, 1034–1051 (2016).
- 630 44. Distler, M. G., Opal, M. D., Dulawa, S. C. & Palmer, A. A. Assessment of behaviors modeling aspects of
631 schizophrenia in *Csmd1* mutant mice. *PLoS One* **7**, e51235 (2012).

632 **Online Methods**

- 633 45. Beck, J. A. *et al.* Genealogies of mouse inbred strains. *Nat. Genet.* **24**, 23–25 (2000).
- 634 46. Ehrich, T. H., Kenney-Hunt, J. P., Pletscher, L. S. & Cheverud, J. M. Genetic variation and correlation of dietary
635 response in an advanced intercross mouse line produced from two divergent growth lines. *Genet. Res.* **85**, 211–
636 222 (2005).
- 637 47. Mayo, L. M. *et al.* Conditioned preference to a methamphetamine-associated contextual cue in humans.
638 *Neuropsychopharmacol. Off. Publ. Am. Coll. Neuropsychopharmacol.* **38**, 921–929 (2013).
- 639 48. Graham, F. K. Presidential Address, 1974. The more or less startling effects of weak prestimulation.
640 *Psychophysiology* **12**, 238–248 (1975).
- 641 49. Elshire, R. J. *et al.* A robust, simple genotyping-by-sequencing (GBS) approach for high diversity species. *PLoS*
642 *One* **6**, e19379 (2011).
- 643 50. Grabowski, P. P., Morris, G. P., Casler, M. D. & Borevitz, J. O. Population genomic variation reveals roles of
644 history, adaptation and ploidy in switchgrass. *Mol. Ecol.* **23**, 4059–4073 (2014).
- 645 51. DePristo, M. A. *et al.* A framework for variation discovery and genotyping using next-generation DNA sequencing
646 data. *Nat. Genet.* **43**, 491–498 (2011).
- 647 52. Korneliussen, T. S., Albrechtsen, A. & Nielsen, R. ANGSD: Analysis of Next Generation Sequencing Data. *BMC*
648 *Bioinformatics* **15**, 356 (2014).
- 649 53. Browning, S. R. & Browning, B. L. Rapid and Accurate Haplotype Phasing and Missing-Data Inference for Whole-
650 Genome Association Studies By Use of Localized Haplotype Clustering. *Am. J. Hum. Genet.* **81**, 1084–1097
651 (2007).
- 652 54. Han, L. & Abney, M. Identity by descent estimation with dense genome-wide genotype data. *Genet. Epidemiol.* **35**,
653 557–567 (2011).
- 654 55. Abney, M. Identity-by-descent estimation and mapping of qualitative traits in large, complex pedigrees. *Genetics*
655 **179**, 1577–1590 (2008).
- 656 56. Browning, B. L. & Browning, S. R. Genotype Imputation with Millions of Reference Samples. *Am. J. Hum. Genet.*
657 **98**, 116–126 (2016).
- 658 57. Chang, C. C. *et al.* Second-generation PLINK: rising to the challenge of larger and richer datasets. *GigaScience* **4**,
659 7 (2015).
- 660

- 661 58. Zhou, X. & Stephens, M. Genome-wide efficient mixed-model analysis for association studies. *Nat. Genet.* **44**,
662 821–824 (2012).
- 663 59. Joo, J. W. J., Hormozdiari, F., Han, B. & Eskin, E. Multiple testing correction in linear mixed models. *Genome Biol.*
664 **17**, 62 (2016).
- 665 60. Han, B., Kang, H. M. & Eskin, E. Rapid and accurate multiple testing correction and power estimation for millions
666 of correlated markers. *PLoS Genet.* **5**, e1000456 (2009).
- 667 61. Schroeder, A. *et al.* The RIN: an RNA integrity number for assigning integrity values to RNA measurements. *BMC*
668 *Mol. Biol.* **7**, 3 (2006).
- 669 62. Degner, J. F. *et al.* Effect of read-mapping biases on detecting allele-specific expression from RNA-sequencing
670 data. *Bioinforma. Oxf. Engl.* **25**, 3207–3212 (2009).
- 671 63. Wang, X. & Clark, A. G. Using next-generation RNA sequencing to identify imprinted genes. *Heredity* **113**, 156–
672 166 (2014).
- 673 64. Kim, D., Langmead, B. & Salzberg, S. L. HISAT: a fast spliced aligner with low memory requirements. *Nat.*
674 *Methods* **12**, 357–360 (2015).
- 675 65. Lawrence, M. *et al.* Software for computing and annotating genomic ranges. *PLoS Comput. Biol.* **9**, e1003118
676 (2013).
- 677 66. Aken, B. L. *et al.* The Ensembl gene annotation system. *Database J. Biol. Databases Curation* **2016**, (2016).
- 678 67. Anders, S. & Huber, W. Differential expression analysis for sequence count data. *Genome Biol.* **11**, R106 (2010).
- 679 68. Pickrell, J. K. *et al.* Understanding mechanisms underlying human gene expression variation with RNA
680 sequencing. *Nature* **464**, 768–772 (2010).
- 681 69. Davis, J. R. *et al.* An Efficient Multiple-Testing Adjustment for eQTL Studies that Accounts for Linkage
682 Disequilibrium between Variants. *Am. J. Hum. Genet.* **98**, 216–224 (2016).
- 683 70. Friddle, C. J. *et al.* High-throughput mouse knockouts provide a functional analysis of the genome. *Cold Spring*
684 *Harb. Symp. Quant. Biol.* **68**, 311–315 (2003).